Characterizing the Decay of Ancient Chinese Silk Fabrics by Microbeam Synchrotron Radiation Diffraction

A. C. Hermes,[†] R. J. Davies,[†] S. Greiff,[‡] H. Kutzke,[§] S. Lahlil,[||] P. Wyeth,[||] and C. Riekel*[,†]

European Synchrotron Radiation Facility ESRF, 6 rue Jules Horowitz, F-38043 Grenoble Cedex, France, Römisch-Germanisches Zentralmuseum, Ernst-Ludwig-Platz 2 D-55116 Mainz, Germany, University of Applied Sciences Cologne, Ubierring 40,D-50678 Köln, Germany, and Textile Conservation Centre, University of Southampton Winchester Campus, Park Avenue, Winchester SO23 8DL, United Kingdom

Received November 1, 2005; Revised Manuscript Received January 1, 2006

Scanning synchrotron radiation microdiffraction with an approximately $1 \times 1\ \mu m^2$ beam has been used as a novel method for characterizing the decay of several T'ang dynasty (618−907 AD) silk fabrics. The crystalline fraction could be visualized based on β-sheet 210 reflection intensities, extracted by recursive peak fits from several thousand diffraction patterns recorded during mesh scans. The azimuthal width of the 210 reflection, which is related to the orientation distribution of the crystalline domains within nanofibrils and the macroscopic orientation of the fibers traversed by the beam, was found to be sensitive to the overall state of decay of the fabric. The fine structure of the histogram of azimuthal width was related to the fiber hierarchical microstructure and the fabric morphology. SAXS/WAXS analysis supports the assumption of an initial loss of the random chain network with decay. At a subsequent state of aging, decay proceeds into the nanofibrils and the silk fibers break up into even smaller fractions.

Introduction

Understanding and quantifying the decay process of silks is of prime importance for the restoration and conservation of silk fabrics. Detailed models of the decay process require an understanding of the effects of light, humidity, or microbes, which are known to be the most damaging factors.[1−4] Experimental techniques such as optical microscopy and scanning electron microscopy (SEM) provide information on the surface morphology of a fabric. Amino acid analysis provides direct evidence for amino acid degradation in old silks.[5] This is interpreted in terms of a preferential decay of the amorphous fraction as observed experimentally from artificially aged silks.[6] For old silks this decay proceeds into the crystalline fraction.[5] Monitoring such degradation processes requires microscopic models derived from X-ray or neutron scattering techniques. Silk fibers spun by spiders and silkworms are known to be hierarchically organized, semicrystalline biopolymers, and microscopic models depend therefore on the hierarchical level considered. Thus, a network of random protein chains, reinforced by nanometer-sized crystalline domains, has been used to model X-ray wide-angle scattering (WAXS) data.[7−10] The crystalline domains in dragline spider silk contain principally $(Ala)_n$ sequences,[11,12] whereas *Bombyx mori* silk contains $(Gly\text{-}Ala)_n$ sequences.[13] X-ray (SAXS) and neutron (SANS) small-angle scattering data on dragline spider silk suggest, however, a more complex morphology of nanofibrils composed of crystalline and short-range order domains within the random chain matrix.[14−16] In view of the similar spinning process and the observation of nanofibrils in *Bombyx mori*,[17] it will be assumed that such a hierarchical model also applies in this case. The change of crystallinity during decay determined by WAXS has been proposed as a measure for the state of decay.[18] The decay of a fabric is, however, a more complex process starting at the level of the fibers (also called single filaments) and propagating through the fabric until the destruction of its morphology. It would therefore be interesting to characterize the state of a silk-fabric by additional parameters relating to the fiber microstructure and the overall state of the fabric. This could provide crucial information with respect to assessing chances of restoration.

In this article scanning synchrotron radiation (SR) microdiffraction[19] is introduced as a novel method for characterizing the state of a silk fabric. This method has already been used for characterizing spider silk threads.[20] The aim of the present study is to derive a composite image ("WAXS-image") of the silk-fabric based on characteristic fitted reflection parameters -such as intensity and width- from an extended area of each archaeological fabric in order to characterize the state of the bulk fabric. The beam size used (about 1 μm) is well below the average size of a single *B. mori* fiber ($<10\ \mu$m)[21] and is therefore sensitive to single fibers. Of particular interest is the analysis of the azimuthal width of the 210 β-sheet reflection, which is related to an axial orientation distribution (Abbr.: OD) of crystalline domains in the fibers.[8,9,22] Decay of the random amorphous protein chain fraction is expected to reduce the network of amorphous chains connecting the crystalline domains and should therefore broaden the OD. A fabric is, however, composed of a multitude of individual fibers, which will show a distribution of orientations in the volume sampled by the X-ray beam. This corresponds to a "macroscopic" OD, which overlays the "microscopic" OD of a single fiber. A degradation of the fabric is therefore expected to introduce an increasing broadening of the "macroscopic" OD through a breaking of the fibers and a loss of fabric coherence. Further information on the decay process is obtained from an analysis of the variation of crystalline and amorphous fractions based on SAXS/WAXS patterns recorded at selected parts of the samples.

* To whom correspondence should be addressed.
[†] European Synchrotron Radiation Facility ESRF.
[‡] Römisch Germanisches Zentralmuseum.
[§] University of Applied Science Cologne.
[||] University of Southampton Winchester Campus.

10.1021/bm0508313 CCC: $33.50
Published on Web 02/25/2006

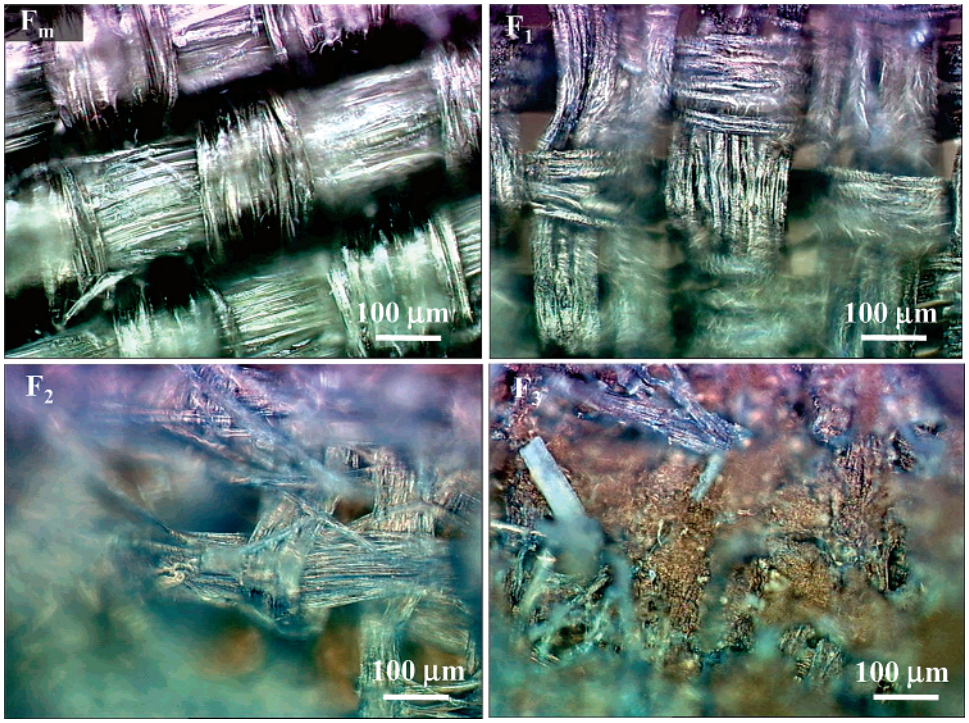

Figure 1. Optical microscopy images of a current plain-weave silk fabric (F_m) and three archeological plain-weave silk fabrics from the Famensi site, classified according to increasing visibility of decay (see text) as F_1, F_2, and F_3.

Materials and Methods

Materials. Several archaeological silk fabrics are investigated in this study, obtained from the Famen temple, China. Detailed sample descriptions are provided elsewhere.[18] The temple is situated 120 km west of the ancient Chinese capital Xi'an and is one of China's most important buddhist sanctuaries. The silk fabrics were part of a treasure once laid down by the T'ang dynasty (618−907 AD) emperors as a gift to the temple. Three plain-weave silk fabrics were selected according to their loss of structural integrity, which was assumed to reflect different states of degradation. In this study the fabrics will be distinguished by their apparent increasing loss of structural integrity as F_1, F_2, and F_3. Optical microscopy images of the fabrics are shown in Figure 1. For comparison, a fabric from a current plain-weave silk fabric (Figure 1-F_m) and an untreated *Bombyx mori* silk thread from a cocoon (B_m; image not shown) are also investigated.

Experiments. SR-microdiffraction experiments were performed at the scanning setup of the ID13 beamline of the European Synchrotron Radiation Facility (ESRF).[19,23] Experiments were performed in air at a temperature of 22 ± 0.5 °C. A focused beam of approximately 1 × 1 μm^2 with <1 mrad divergence was generated by crossed mirror optics. The wavelength of the monochromatic beam was $\lambda = 0.0975$ nm. Samples were glued to tapered glass capillary tips, and 2D raster scans were performed in transmission geometry. At every raster point, an X-ray pattern was recorded by a 16-bit readout CCD detector with X-ray converter screen. The measuring time per pattern was between 1 and 5 s. A typical raster scan covered an area of 50 × 50 μm^2 with 1 × 1 μm^2 raster steps (2500 X-ray patterns). The silk thread was scanned over an area of 50(vert) x 5000(hor)μm^2 with raster steps of 2.5(vert) × 50(hor) μm^2 (2000 X-ray patterns). The output of an ionization chamber in front of the sample was used to scale the patterns in each series. The lower Q limit ($Q = 2\pi d^{-1}$; where d is a lattice spacing), defined by the beam divergence and beamstop, was typically $Q_{min} = 1.24$ nm^{-1} ($d_{max} = 5.07$ nm), whereas the upper Q limit, defined by the detector size and the detector-to-sample distance, was typically $Q_{max} \leq 40$ nm^{-1} ($d_{max} \approx 0.157$ nm). The lower Q limit did not allow higher resolution SAXS experiments, but extended tails of SAXS curves could be observed.

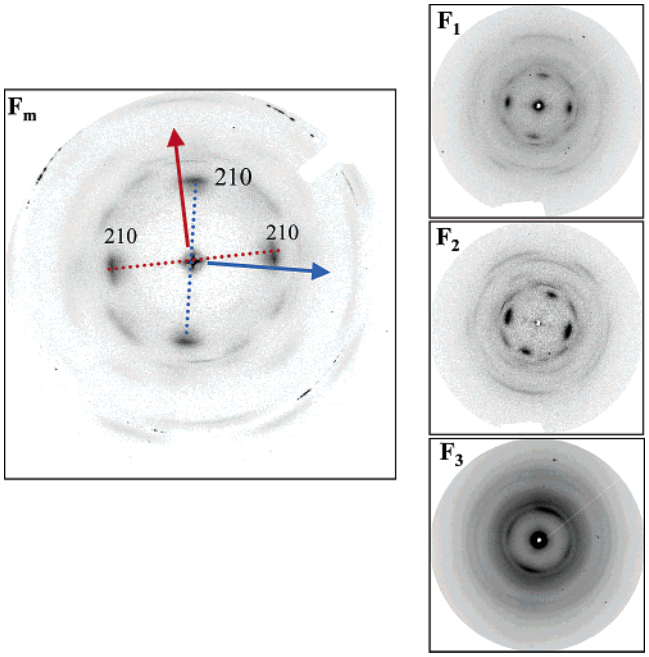

Figure 2. Diffraction pattern from the different silk fabrics obtained in an area where the two major fiber orientations in the fabric overlap. The equatorial pattern with the dominating 210 reflection is therefore doubled. This doubling is still present in the F_3 sample, which shows optically the most advanced degree of decay (Figure 1). The two equators and the corresponding fiber axis orientations are indicated in red and blue for the F_m pattern.

Optical microscopy was performed with an Olympus BX51WI microscope with long working distance objectives (LMPFL series; ≤50×), integrated into the scanning setup.[23] The microscope was located downstream from the sample and had to be moved out of the X-ray beam path during data collection. As compared to imaging with an on-axis, pierced zoom-objective,[24] a higher resolution and a better image quality can thus be obtained. The position of the beam on the

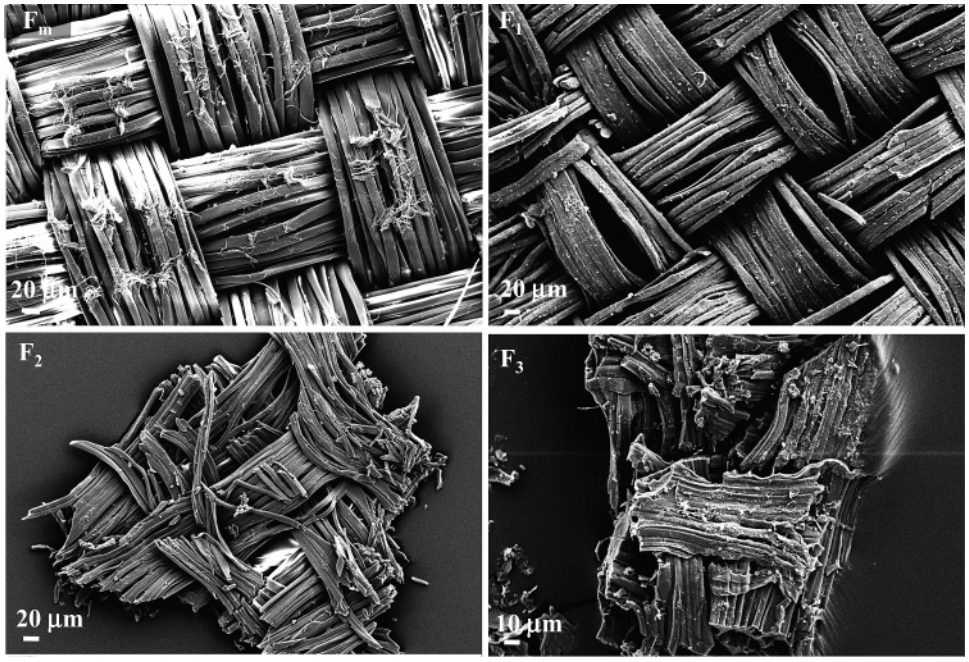

Figure 3. SEM images of F_m, F_1, F_2, and F_3 samples. Note that the sample areas displayed do not correspond to the areas scanned by the SR-beam (Figure 4A,B). The small fibrils in the F_1 image are due to wear effects.

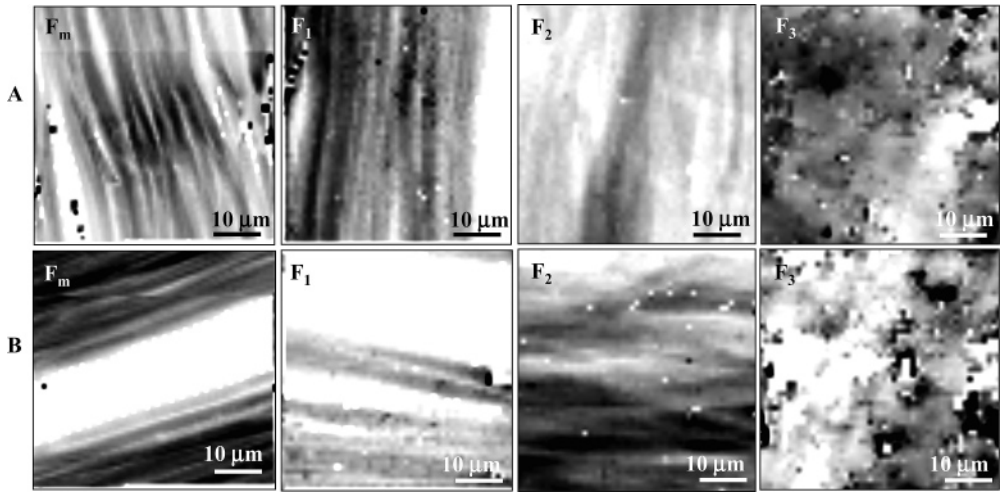

Figure 4. Rows A and B: Composite scanning diffractometry images, based on integrated intensity of the 210 reflection (I_{rel}), showing the two main fiber-orientations in the fabrics. Size of composite images: 50×50 μm^2 with 1×1 μm^2 pixel size. Note that the scales of the optical (Figure 1) and composite images differ. Empty space is indicated by white color and increasing scattering intensity by a darkening.

sample was calibrated to about 2 μm precision by scattering from two orthogonal polymer fibers. Images were recorded by a CCD camera with analogue readout and digitized by a Matrox video processor.

Scanning electron microscopy (SEM) was performed off-line with a LEO 1530 field emission SEM (10 keV). The sample area images did therefore not correspond to the sample area investigated by optical microscopy. The F_3 sample had in particular disintegrated into fragments and the fragments imaged were arbitrarily selected according to the remaining fabric morphologies.

Data Reduction. The diffraction patterns obtained in an area where the two major fiber orientations in a fabric overlap show a cross pattern of equatorial 210 reflections. (Figure 2) The local fiber orientations are orthogonal to the orientation of the respective equators and are indicated by blue and red arrows in Figure 2-F_m. The 210 reflection corresponds to the β-sheet structure interchain distance of the orthogonal *B. mori* unit cell.[13] The cross pattern was observed in all fabrics including the F_3 sample, which shows optically the highest state of decay and has therefore retained a memory of the original fabric. (Figure 1-F_3).

WAXS images were obtained by recursive data analysis of the 210 reflections obtained for each complete raster scan using a combination of the FIT2D software[25] and custom-made batch analysis software. The azimuthal intensity distribution was generated by radial integration across the reflection profile. The azimuthal intensity distribution was fitted by Gaussian functions for the Bragg peaks. The treatment of background was approximated by polynomials for the recursive fits, whereas more refined modeling of selected diffraction patterns can be based on several Gaussians or other functions of different width.[8,9] For the *B. mori* thread, the background showed a broad peak at the 210 reflection position and was fitted by a 2nd order polynomial. For the F_1 and F_2 samples, the background did not show a peak and was fitted by a 0 order polynomial. The tilted F_3 background required a 1st order polynomial. The fitted Gaussian profile parameters, reflection width (^{0}full-width-half-maximum; ^{0}fwhm) and integrated relative intensity (I_{rel}), were used for further analysis. The 210 reflection width is correlated with the axial OD of crystalline domains[8,9,22] and will be used instead of an OD value. Display and curve fitting of histograms were based on OriginPro (OriginLab).

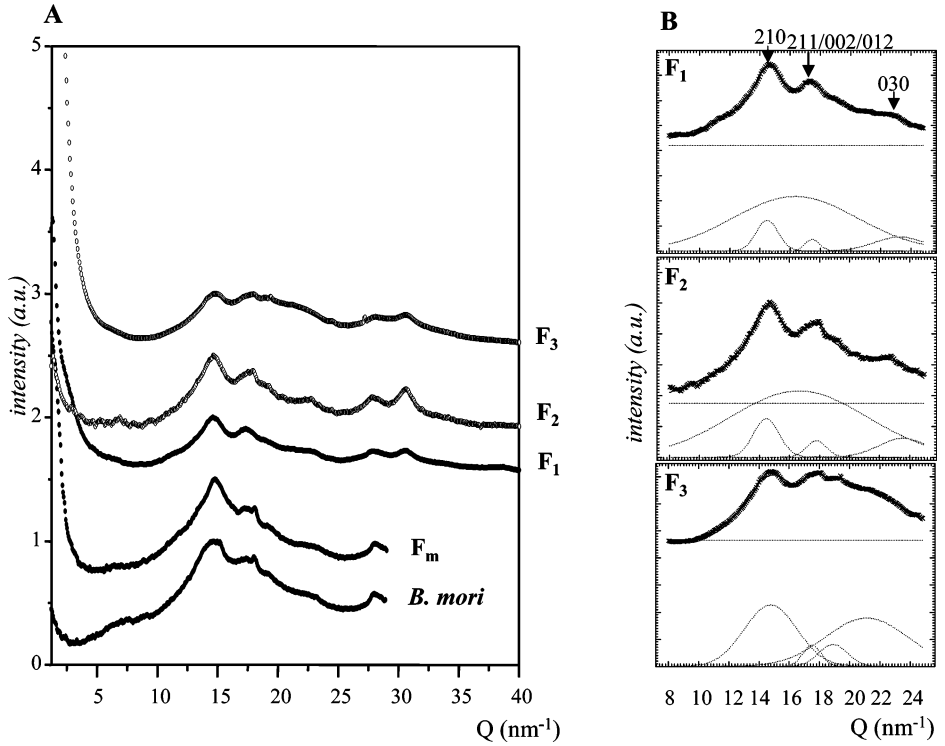

Figure 5. (A) 1D intensity profiles calculated by azimuthally averaging selected 2D diffraction patterns through 360°; $Q = 4\pi \sin\Theta\lambda^{-1} = (2\pi)/d$ where Θ is the Bragg angle and d the lattice spacing. Data for *B. mori* thread and the F_m sample were recorded at different experimental conditions than for F_1, F_2, and F_3. The individual curves have been normalized to the maximum intensity of the 210 reflection (=1.0) and shifted vertically by 0.5 intensity unit increments for better visualization. Solid circles: *B. mori*, F_m and F_1; open circles: F_2 and F_3. (B) Gaussian profile fits of F_1, F_2, and F_3 intensity profiles for $8 < Q < 25$ nm^{-1} range (blue curves). Reflection indices according to ref 36.

Results and Discussion

Visualization of Fabrics. Optical microscopy shows that fabric degradation, as evidenced by broken fibers and a partial loss of the plain-weave morphology, becomes noticeable for the F_2 sample (Figure 1). The F_3 sample shows no longer a plain-weave morphology but only a conglomerate of smaller fiber pieces. The higher resolution SEM images show more morphological details (Figure 3). The F_m sample shows some sign of wear (loose fibrils) but the individual fibers are not broken. The F_1 sample already shows a few fractured fibers. The F_2 sample contains as expected a significantly higher amount of fractured fibers together with shorter fiber segments. The F_3 sample has disintegrated into small fragments, which however, still show some remnants of the plain-weave morphology and the fiber structure. Fibers seem, however, to have fused together, which has also been observed after microbial degradation.[4]

In contrast to optical microscopy and SEM, which show only the surface morphology, WAXS imaging provides information on the bulk crystalline fraction (Figure 4). The two major fiber orientations can be visualized in projection by selecting alternatively the 210 reflection I_{rel} values from the two equatorial directions of the cross pattern. (Figure 2). Each pixel of the composite WAXS-image corresponds to an I_{rel} value. We note that several individual fibers are resolved in the F_m and F_1 samples and to a lesser degree in the F_2 sample. The F_3 sample is seen to be in an advanced state of decay, as extended fibers cannot be distinguished. The visualization of the bulk crystalline fraction by WAXS imaging provides therefore similar information on the state of the fabric as optical microscopy and SEM.

Intensity Profile Analysis. In order to further verify the assumption of a preferential loss of amorphous fraction during the first steps of decay,[18] 1D intensity profiles were calculated by azimuthally averaging selected 2D-diffraction patterns through 360°. Crystallinity is present for all samples. We note, however, that the Bragg reflections are particularly well defined up to the highest Q values for the F_2 sample, which suggests qualitatively that this sample has the highest crystallinity (Figure 5A). A more detailed analysis can be based on Gaussian fits to the intensity profile in the range $8 < Q < 25$ nm^{-1} (Figure 5B). It is interesting to note that a broad diffuse peak at $Q \approx 16.4$ nm^{-1} exists for the F_1 and F_2 samples, whereas this peak has disappeared for the F_3 sample and has been replaced by a diffuse peak at $Q \approx 21.1$ nm^{-1} due to amorphous decay products. The $Q \approx 16.4$ nm^{-1} diffuse peak, which is present in all samples but the F_3 sample, is assigned to the short-range order domains of semicrystalline nanofibrils as for spider dragline silk.[8,14−16,26] The persistence of short-range order domains for the F_1 and F_2 samples suggests that a loss in amorphous fraction is limited to the random chain matrix. The SAXS range should be sensitive to this decay model as the SAXS intensity is proportional to the electron scattering density difference between the semicrystalline nanofibrils and the random chain matrix.[14−17,26−28] The low Q range of selected 2D patterns of all silk materials is shown in Figure 6A. We note the strong equatorial streak in the *B. mori* sample, which is also present in dragline silk and can be related to the electron density contrast ($\Delta\rho^*$) between semicrystalline nanofibrils (ρ_n) and random chain matrix (ρ_a).[14,16] The intensity of the equatorial streak can be written as $I(Q) = k'P_n(Q)\Delta\rho^*$, where P_n is the nanofibrils form factor and k' is a constant.[16] Both the F_m and F_1 samples show an additional unoriented low-angle background, which could be due to additives (e.g., colorants) absorbed by the random chain matrix. The reduction of the SAXS intensity close to the beamstop for the F_2 sample is striking and can be explained in the frame of the nanofibrillar model by a reduction

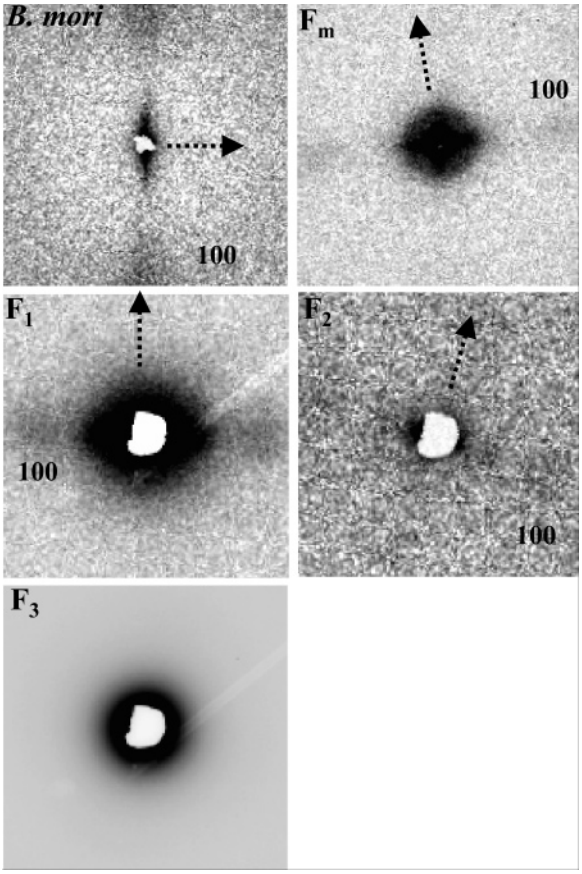

Figure 6. Zoom into low-angle scattering range ($Q_{max} = 7.42$ nm^{-1}). The position of the 100 reflection and the orientation of the meridian are indicated. The size of the beamstop was in each case about 300 μm diameter. The apparent size on the detector differs, however, for the *B. mori* and F_m samples from the other samples due to a different distance beamstop-to-sample.

of the $\Delta\rho^*$ term. Replacing the ρ_a term by empty space would, however, still imply a strong $\Delta\rho^*$ contrast term. It is therefore probable that the loss of random chain matrix results in a collapse of neighboring nanofibrils so that the $\Delta\rho^*$ term is suppressed. The strong increase of the SAXS signal for the F_3 sample is attributed to scattering from nanometer-sized crystalline domains, similar to that found for carbon black. These crystalline domains result from a preferential decay of the short-range order domains in the nanofibrils. The residual crystallinity due to the domains is seen in the F_3 WAXS pattern (Figure 5A,B). The observation that the diffuse WAXS peak has disappeared in the F_3 sample agrees also with the assumption that the short-range order domains of the semicrystalline nanofibrils have been destroyed.

Reflection Width Analysis. A more detailed view of the bulk fabric decay could be obtained by monitoring the evolution of the 210 reflection width for the different fabrics. For comparison, benchmark values were determined for the *B. mori* thread. A WAXS image of I_{rel} values of the thread reveals a cylindrical twisting of the two fibers, which can be distinguished at the positions, marked by arrows (Figure 7A). The corresponding 210 width distribution across the thread is shown in Figure 7B. The color-coded intensity scale corresponds to the width of the histogram peak discussed below (Figure 8). As a sidenote, we note that the narrow zones of higher width values might be related to an increased local stress due to the head movement of the silkworm or from some other part of the spinning organ.[29,30] Thus, we note that the modulation of the reflection width during dragline spinning might reflect a mechanical action of the spinneret on the nascent fiber.[31]

The spatial distribution of 210-width values was used to create a histogram of width distribution in bins of 0.25°. The histograms based on the vertical and horizontal fibers of each fabric are similar in width and position relative to the *B. mori* benchmark values. For further data analysis, both orientations were therefore averaged. The frequencies of each sample series have been normalized to the sum of frequencies so that the peak areas are the same (Figure 8). We note the broadening and the shift of the histograms to larger width values, in particular for the archeological samples. This corroborates qualitatively that the F_1 sample has suffered only a limited amount of decay, whereas the loss in integrity is already in an advanced state for the F_2 sample as evidenced by the tail extending to higher width values. The F_3 sample has reached the most advanced state of decay and the strong diffuse scattering halo suggests an important amorphous fraction originating from the decomposition of the crystalline fraction. Interestingly, the modern silk

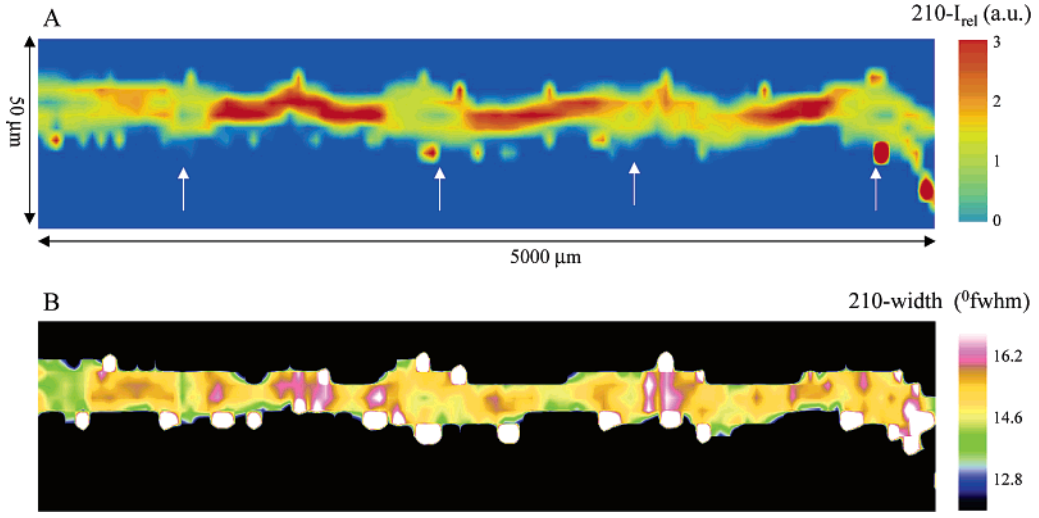

Figure 7. (A) composite plot of I_{rel} distribution of the 210 reflection across the *B. mori* thread. The thread was cylindrically twisted so that the two individual fibers can only be seen at the positions marked by white arrows. Real size of composite image: 50 × 5000 μm^2 with 2.5 × 50 μm^2 pixel size. (B) Composite plot of the azimuthal width of the 210 reflection across the thread. The width-scale from 12° to 16° fwhm is color-coded and covers the full peak range in the *B. mori* histogram (Figure 8). The white spots correspond to fwhm values outside of the color scale, which are due to a low counting statistics.

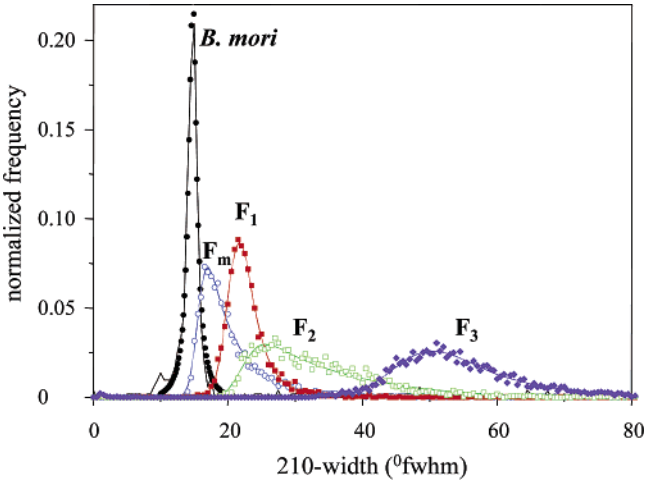

Figure 8. Experimental data (symbols) and fitted functions (solid lines) of histograms of 210-width distribution. The frequencies of each sample-series have been normalized to the sum of frequencies. Each bin corresponds to 0.25°; *B. mori* thread (Lorentzian function; black); F_m(blue), F_1(red), F_2(green), and F_3(violet): exponentially modified Gaussian functions

Table 1. Peak Fit Parameters of the Histograms[a]

	L	G_m			
fit-parameter	*B. mori*	F_m	F_1	F_2	F_3
P_0	14.76 (2)	15.58 (4)	20.38 (4)	22.3 (2)	45.8 (2)
W_0	1.4 (1)	2.0 (8)	2.3 (1)	4.1 (2)	9.2 (4)

[a] Error estimations in brackets. *L*, Lorentz-function; G_m, exponentially modified Gaussian. P_0 and W_0 are the position (0) and width (0fwhm) of the deconvoluted Gaussian peaks.

fabric (F_m) histogram is already shifted in position relative to the *B. mori* thread value (Figure 8). The origin of this effect is currently not understood but could be to the loss of sericin coating in the silk fabric, which has been shown to have an influence on the defect distribution in silk.[21] The low-angle components in the F_m and F_1 patterns could be due to organic dye molecules incorporated into the amorphous phase (Figure 5). The resulting modified network properties could also result in an increase in the OD.

The symmetric shape of the *B. mori* histogram peak can be fitted by a Lorentzian profile. The fabric-histogram peaks are, however, more or less tailed, which is probably due to the angular spread of fiber orientations along the beam path overlaying the single fiber OD. These histograms could be fitted by an exponentially modified Gaussian profile, used also in chromatography[32] (Figure 8). A deconvoluted Gaussian peak position could thus be derived with the profile parameters position (P_0) and width (W_0) collected in Table 1. The shape of the fabric histogram peaks suggests a convolution of a microscopic term due to the OD of a fiber and a macroscopic term due to the angular spread of fibers sampled along the SR-beam path. The deconvoluted Gaussian width, W_0, is tentatively attributed to the microscopic term, which implies that the shift of the peak position (P_0) with increasing decay is due to a disordering of crystalline domains in a fiber. It is interesting to note that the F_m sample has a more extended tail as compared to that of the F_1 sample. We speculate that surface wear evident in the F_m SEM images (Figure 3) results in a fraction of fibers showing the higher macroscopic term. We also note that the P_0 values of the F_1 and F_2 samples are similar and much smaller than the P_0 value of the F_3 sample, which suggests a fraction of fibers of similar deterioration state in the F_1 and F_2 samples. The strong F_2 tail extending to larger width values suggests, however, an additional fraction with a more advanced state of decay. This is probably due to a break up of the fibers as shown in the SEM-images. (Figure 3) The value of $P_0 = 45.8$ suggest, however, the existence of an F_3 fiber fraction containing highly disordered crystalline domains. The origin of this disordering must be due to the loss of amorphous network connecting the crystalline domains. The remaining nanofibrils[17] are more free to axial disorder. An analogous breakdown of the amorphous chain network is assumed for spider dragline silk due to water absorption.[10,33] Thus, the azimuthal width of the 210 β-sheet reflection[13] of 17−18° fwhm in dry silk[9] rises to 30−40° in hydrated (supercontracted) silk,[34] which is in the range of the P_0 value for the F_3 sample.

Conclusions

Scanning synchrotron radiation microdiffraction has been used to characterize the microstructure of silk fabrics in various states of decay. "WAXS imaging" based on fitted 210 β-sheet reflection parameters, such as integrated intensity and azimuthal width, is complimentary to optical microscopy and SEM studies, which visualize the surface morphology of materials. The coverage of an extended area allows a statistically significant number of fibers to be sampled. The azimuthal width of the 210 reflection appears to be a sensitive indicator for the state of decay. The histogram of azimuthal width distribution is found to be symmetric for the silk thread and asymmetric for the fabrics, which has been related to a convolution of the axial OD of crystalline domains in the nanofibrils and the fabric morphology. A method of extracting a symmetric term peak due to the fiber microstructure by a Gaussian deconvolution is proposed. An increasing decay appears to broaden the symmetric term peak and shift the peak center to larger values, presumably due to a loss of the connecting amorphous network. SEM shows a fractioning of fibers into shorter segments with increasing decay. This introduces disorder, which could explain the increasing tails of the histograms. SAXS/WAXS data obtained at selected positions support an onset of decay in the fibers by a loss of random protein chains. At a subsequent stage of aging, cleavage proceeds into the nanofibrils and the silk fibers break up into even smaller fragments. Restorative action requires probably that the nanofibrillar morphology remains largely intact and can be embedded in an artificial random polymer chain matrix. Similar studies could be performed for a range of fabrics and tissues and could be applied to the structural mechanics of fibers and fabrics.[35]

Acknowledgment. The support by BMBF and the German Ministry of Education and Research for funding the silk project is gratefully acknowledged. We thank I. Snigireva (ESRF) for providing the SEM images. M. Burghammer (ESRF) helped during the alignment of the ID13 beamline.

References and Notes

(1) Miller, J. E.; Reagan, B. M. *J. Am. Inst. Conserv.* **1989**, *28*, 97−115.
(2) Kuruppilai, R. V.; Hersh, S. P.; Tuecker, P. A. In *Historic Textile and Paper Materials: Conservation and Characterization*; Needles, H. K., Zeronian, S. H., Eds.; American Chemical Society: Washington DC, 1986; Vol. 212, pp 111−127.
(3) Leene, J. E.; Demeny, L.; Elema, R. J.; DeGraff, A. J.; Surtel, J. In *Proceedings of the International Council of Museums*, 1958; Vol. 13, pp 107−242.
(4) Seves, A.; Romano, M.; Maifreni, T.; Sora, A.; Ciferri, O. *Int. Biodeterior. Biodegrad.* **1998**, *42*, 203-211.
(5) Becker, M. A.; Magoshi, Y.; Sakai, T.; Tuross, N. C. *Stud. Conserv.* **1997**, *42*, 27−37.

(6) Becker, M. A.; John Hopkins University: Ann Arbor, 1997.
(7) Kaplan, D.; Adams, W. W.; Farmer, B.; Viney, C., Eds. *Silk Polymers; Materials Science and Biotechnology*; Americal Chemical Society: Washington, DC, 1994; Vol. 544.
(8) Grubb, D. T.; Jelinski, L. W. *Macromolecules* **1997**, *30*, 2860−2867.
(9) Riekel, C.; Bränden, C.; Craig, C.; Ferrero, C.; Heidelbach, F.; Müller, M. *Int. J. Mol. Biol.* **1999**, *24*, 187−195.
(10) Termonia, Y. *Macromolecules* **1994**, *27*, 7378−7381.
(11) Simmons, A.; Michal, C.; Jelinski, L. *Science* **1996**, *271*, 84−87.
(12) Lewis, R. V. *Acc. Chem. Res.* **1992**, *25*, 392−398.
(13) Fraser, R. D. B.; MacRae, T. P. *Conformations of Fibrous Proteins*; Academic Press: New York, 1973.
(14) Yang, Z.; Grubb, D. T.; Jelinski, L. W. *Macromolecules* **1997**, *30*, 8254−8261.
(15) Riekel, C.; Vollrath, F. *Int. J. Mol. Biol.* **2001**, *29*, 203-210.
(16) Sapede, D.; Seydel, T.; Forsyth, T.; Koza, M. M.; Schweins, R.; Vollrath, F.; Riekel, C. *Macromolecules* **2005**, *38*, 8447−8453.
(17) Putthanarat, S.; Stribeck, N.; Fossey, S. A.; Eby, R. K.; Adams, W. W. *Polymer* **2000**, *41*, 7735−7747.
(18) Greiff, S.; Kutzke, H.; Lahlil, S.; Riekel, C.; Wyeth, P. In *AHRC Research Centre for Textile Conservation and Textile Studies First Annual Conference*; Janaway, R., Wyeth, P., Eds.; Archetype Publications Ltd.: London, 2004; pp 38−43.
(19) Riekel, C. *Rep. Prog. Phys.* **2000**, *63*, 233−262.
(20) Riekel, C.; Craig, C. L.; Burghammer, M.; Müller, M. *Naturwissenschaften* **2001**, *88*, 67−72.
(21) Perez-Rigueiro, J.; Elices, M.; Llorca, J.; Viney, C. *J. Appl. Polym. Sci.* **2001**, *82*, 1928−1935.
(22) Stein, R. S.; Wilkes, G. L. In *Structure and Properties of Oriented Polymers*; Ward, I. M., Ed.; Applied Science Published Ltd.: London, 1975; pp 57−145.
(23) Riekel, C.; Burghammer, M.; Schertler, G. *Curr. Opin. Struct. Biol.* **2005**, *15*, 556−562.
(24) Riekel, C. *J. Synchrotron Radiat.* **2003**, *11*, 4−6.
(25) Hammersley, A. In *http://www.esrf.fr/computing/scientific/FIT2D/*.
(26) Burghammer, M.; Müller, M.; Riekel, C., Eds. *X-ray synchrotron radiation microdiffraction on fibrous biopolymers such as cellulose and in particular spider silks*; Research Signpost: Trivandrum, India, 2003; Vol. 7.
(27) Londono, D.; Annaduari, V.; Gopalkrishna, R.; Okuyama, K.; Somashekar, R. *J. Polym. Mater.* **2002**, *19*, 7−12.
(28) Londono, J. D.; Annadurai, V.; Gopalkrishne, R.; Somashekar, R. *J. Appl. Polym. Sci.* **2002**, *85*, 2382−2388.
(29) Miura, M.; Pan, Z. J.; Aoyama, S.; Morikawa, H.; Mochizuki, S. *J. Seric. Sci. Jpn* **1998**, *67*, 51−56.
(30) Shao, Z.; Vollrath, F. *Nature* **2002**, *418*, 741.
(31) Riekel, C.; Müller, M.; Vollrath, F. *Macromolecules* **1999**, *32*, 4464−4466.
(32) Sternberg, J. C. *Advances in Chromatography*; Marcel Dekker: New York, 1966; Vol. 2.
(33) Work, R.; Morosoff, N. *Textile Res. J.* **1982**, 349−356.
(34) Grubb, D. T.; Ji, G. *Int. J. Mol. Biol.* **1999**, *24*, 203-210.
(35) Hearle, J. W. S., Grosberg, P., Backer, S., Eds.; *Structural Mechanics of Fibers, Yarns, and Fabrics*; Wiley-Interscience: New York, 1969; Vol. 1.
(36) Marsh, R. E.; Corey, R. B.; Pauling, L. *Biochim. Biophys. Acta* **1955**, *16*, 1−34.

BM0508313